The EMBO Journal Vol. 21 No. 14 pp. 3598–3607, 2002

Conformational changes in surface structures of isolated connexin 26 gap junctions

Daniel J.Müller[1,2,3], Galen M.Hand[4], Andreas Engel[5] and Gina E.Sosinsky[3,4,6]

[1]Max Planck Institute of Molecular Cell Biology and Genetics, Dresden, [2]BIOTEC, Technical University Dresden, Dresden, Germany, [4]National Center for Microscopy and Imaging Research, Department of Neurosciences, [6]San Diego Supercomputer Center, University of California, San Diego, La Jolla, CA, USA and [5]M.E.Müller Institute for Structural Biology, Biozentrum, Basel, Switzerland

[3]Corresponding authors
e-mail: mueller@mpi-cbg.de or gsosinsky@ucsd.edu

Gap junction channels mediate communication between adjacent cells. Using atomic force microscopy (AFM), we have imaged conformational changes of the cytoplasmic and extracellular surfaces of native connexin 26 gap junction plaques. The cytoplasmic domains of the gap junction surface, imaged at submolecular resolution, form a hexameric pore protruding from the membrane bilayer. Exhibiting an intrinsic flexibility, these cytoplasmic domains, comprising the C-terminal connexin end, reversibly collapse by increasing the forces applied to the AFM stylus. The extracellular connexon surface was imaged after dissection of the gap junction with the AFM stylus. Upon injection of Ca^{2+} into the buffer solution, the extracellular channel entrance reduced its diameter from 1.5 to 0.6 nm, a conformational change that is fully reversible and specific among the divalent cations tested. Ca^{2+} had a profound effect on the cytoplasmic surface also, inducing the formation of microdomains. Consequently, the plaque height increased by 0.6 nm to 18 nm. This suggests that calcium ions induce conformational changes affecting the structure of both the hemichannels and the intact channels forming cell–cell contacts.

Keywords: calcium/connexon/intercellular communication/ion channel structure/membrane protein structure

Introduction

Gap junctions are the sites of direct cell-to-cell communication in vertebrates, facilitating the exchange of molecules and signals. These intercellular channels are pairs of hexameric half-channels, called connexons or hemichannels, which are connected coaxially to bridge the extracellular space between two adjacent plasma membranes. Thousands of docked connexon pairs are tightly packed into junctional plaques that are planar, double-layered structures with distinct boundaries. Connexons are assembled from one or more connexins, which are a family of highly conserved polypeptides. At present, 21 members of this family have been identified in mammals and more have been identified in non-mammalian vertebrates that are orthologs of these mammalian isoforms (Willecke *et al*., 2002). Connexins exhibit a conserved core comprising the N-terminus, four transmembrane domains and two extracellular loops, as well as a variable portion consisting of the cytoplasmic loop and C-terminus.

The three-dimensional (3D) structure of recombinant gap junction channels derived from cryo-electron microscopy at a resolution of 7 Å has recently provided direct evidence for α-helical folding of four transmembrane domains within each connexin subunit (Unger *et al*., 1999). Complementary to electron microscopy (EM), atomic force microscopy (AFM; Binnig *et al*., 1986) provided the first insight into the connexon extracellular surface structure (Hoh *et al*., 1991, 1993). Sample preparation and imaging procedures of AFM have been improving steadily, thereby allowing surface structures of native proteins to be observed at a vertical resolution of 0.1 nm and a lateral resolution of <1 nm (Engel *et al*., 1997; Czajkowsky and Shao, 1998). Most attractive for biologists, AFM reveals the biological object in buffer solution, at ambient temperatures and with an outstanding signal-to-noise ratio, allowing observation of single proteins at work in their native environment (Engel *et al*., 1999; Engel and Müller, 2000).

Early experiments measuring cell–cell coupling in several cell systems have shown that Ca^{2+} ions decrease or suppress electrical coupling mediated by gap junctions (Loewenstein *et al*., 1967; Oliveira-Castro and Loewenstein, 1971; DeMello, 1975). These observations and other experiments formed the basis of Loewenstein's 'calcium hypothesis', which states that cytoplasmic calcium ion levels regulate the gating of gap junction channels (Loewenstein, 1966). Large fluxes of cytoplasmic calcium ion concentrations have long been postulated as a cellular apoptotic mechanism that uncouples the gap junctions in dying cells, thereby isolating dying cells from healthy neighbors. Following up on Loewenstein's hypothesis, Unwin and colleagues published two EM structures of isolated rat liver gap junctions at ~2.5 nm resolution, one prepared in the presence of calcium ions, the other prepared in the presence of calcium ion chelators (Unwin and Zampighi, 1980; Unwin and Ennis, 1984). Their interpretation of the differences between the Ca^{2+} and Ca^{2+}-free structures lead them to postulate that Ca^{2+} ions cause a rotation of the subunits that closes the pore in a manner analogous to the closing of a camera iris. However, while calcium-mediated uncoupling has been studied since the 1960s, we still do not understand this effect, and neither can we resolve the puzzle of cells producing calcium waves that are transmitted from cell to cell (Rottingen and Iversen, 2000). Nevertheless, recent studies show that cells containing high concentrations (~1–2 mM) of calcium ions in the external medium may

close non-junctional gap junction hemichannels [connexin (Cx) 43 (Li *et al*., 1996); Cx46 (Pfahnl and Dahl, 1999); and Cx26 (Kamermans *et al*., 2001)].

Here we report the first high-resolution topographs of both connexon surfaces and their conformational changes. The cytoplasmic C-terminal domains form a hexameric pore exhibiting a high degree of structural flexibility. Upon increasing the force applied to the AFM stylus by a few tens of picoNewtons (1 pN = 10^{-12} N), these domains reversibly collapse onto the membrane surface. Concomitant with these considerable structural rearrangements, the cytoplasmic channel entrance appears to close. We demonstrate that in single connexon layers, the hexameric extracellular pore appears more rigid, with its channel entrance narrowing significantly in the presence of Ca^{2+} ions. A different structural change is observed with intact gap junctions upon calcium ion incubation. Our results demonstrate that the Ca^{2+}-induced closure of gap junction hemichannels is the result of a change in conformation in the pore opening at the extracellular surface. Furthermore, the results presented here indicate that there is a different gating mechanism for closure at the extracellular surface from the one that occurs at the cytoplasmic surface. Therefore, two distinct structural entities within the connexon are likely to act as physical gates at the two ends of the pore.

Results

Imaging and dissection of gap junction plaques

Gap junction plaques adsorbed to freshly cleaved mica and recorded in buffer solution by AFM (Figure 1A, marked as GJ) exhibited a thickness of 17.4 ± 0.7 nm (n = 47). In contrast, the lipid membranes (Figure 1A, marked as LM) surrounding the protein membranes had a height of 4.5 ± 0.5 nm (n = 58), while single layered connexon membranes (Figure 1A, marked as CX) showed a height of 8.0 ± 0.6 nm (n = 24). A summary of these thickness measurements is shown in Table I.

As visible from the overview image, only small regions of the extracellular surface were exposed to the AFM stylus (Figure 1A, marked as CX). To image a larger area of this interface, the upper connexon layer was removed carefully using the AFM stylus as a 'nanotweezer' (Figure 1B and C) (Hoh *et al*., 1991; Schabert *et al*., 1995; Fotiadis *et al*., 1998, 2000, 2002). Following this, the extracellular surface of the remaining single-layered connexon membrane was imaged at higher magnification and the hexagonal assembly of individual connexons into microcrystalline patches became visible (Figure 1D).

Because the forces used for AFM image recording were not destructive to the specimen, the same gap junction or connexon layer can be imaged repeatedly. This was a prerequisite to observe reproducible structural changes of the membrane surface. Additionally, comparing membrane surfaces imaged using the same AFM stylus minimized possible errors arising from tip artifacts (Schwarz *et al*., 1994).

Cytoplasmic domains of the gap junction form a hexagonal pore

Imaged at a higher resolution and with the minimum force applied to the AFM stylus (50 ± 20 pN) to obtain stable images, the cytoplasmic gap junction surface (Figure 1A, GJ) exhibited donut-shaped structures assembled into a hexagonal lattice, with a unit cell distance of 7.7 ± 0.5 nm (Figure 2A, top). Such imaging conditions were obtained after carefully balancing electrostatic repulsion and van der Waals attraction between stylus and protein (Müller *et al*., 1999a). While individual connexons are distinct in the unprocessed topograph, their consistent structural features are revealed by their average (Figure 2B). Each gap junction exhibited six protruding cytoplasmic domains, forming a donut-like structure. The donuts had an outer diameter 5.6 ± 0.3 nm (n = 68) at full width half maximum (FWHM), and their pores had an inner diameter of 2.8 ± 0.3 nm (n = 68) with a depth of 1.0 ± 0.3 nm (n = 30). In the average structure, the cytoplasmic domains protruded by 1.7 ± 0.2 nm (n = 30) from the lipid bilayer (Figure 2B, +). A summary of these pore dimensions is shown in Table I.

Cytoplasmic gap junction surface domains exhibit high structural flexibility

When imaged with a slightly enhanced force applied to the stylus (70 ± 20 pN), the cytoplasmic domains were observed to collapse onto the membrane surface (Figure 2A, center to bottom). This structural change was fully reversible and could be repeated several times without detectable structural destruction. The collapse of the cytoplasmic domains formed a supra-structure on the membrane surface (Figure 2C) that reduced the gap junction thickness by 1.5 nm. Consequently, these surface structures protruded only 0.2 ± 0.2 nm (n = 30) above the lipid bilayer (Figure 2C, cross). The cytoplasmic domains of this conformation surrounded an enlarged channel entrance exhibiting an inner diameter of 4.7 ± 0.3 nm (n = 27) at FWHM and formed a pore (asterisks) with an outer diameter of 5.8 ± 0.3 nm (n = 27). The depth of the pore was ~1.6 ± 0.2 nm (n = 27), while the center-to-center distance of the unit cell (7.7 ± 0.5 nm) remained unchanged.

Extracellular connexon surface structure

When imaging the extracellular connexon surface in the Ca^{2+}-free buffer used for isolation at high magnification (pixel size <0.4 nm), the extracellular domains of the individual connexons were distinctly visible (Figure 3). The six subunits protruding by 1.6 ± 0.2 nm (n = 57) above the lipid bilayer are arranged into a donut-shaped structure surrounding a central pore. The donuts exhibited a FWHM outer diameter of 4.9 ± 0.3 nm and the pore had an inner diameter of 1.3 ± 0.3 nm with a depth of 1.0 ± 0.2 nm (n = 108). Single connexins were sometimes missing (Figure 3A, circles), which is likely due to the mechanical dissection of the gap junction plaques (also seen in lower resolution images in Hoh *et al*., 1993). The gap junction plaques and single connexon layers investigated exhibited well ordered, as well as less ordered regions. When measured in the crystalline areas, the center-to-center distance of connexons at the extracellular surface did not show significant deviations from that measured on intact channels on the cytoplasmic surface. This distance is dependent on the crystallinity of the lattice rather than the surface being imaged.

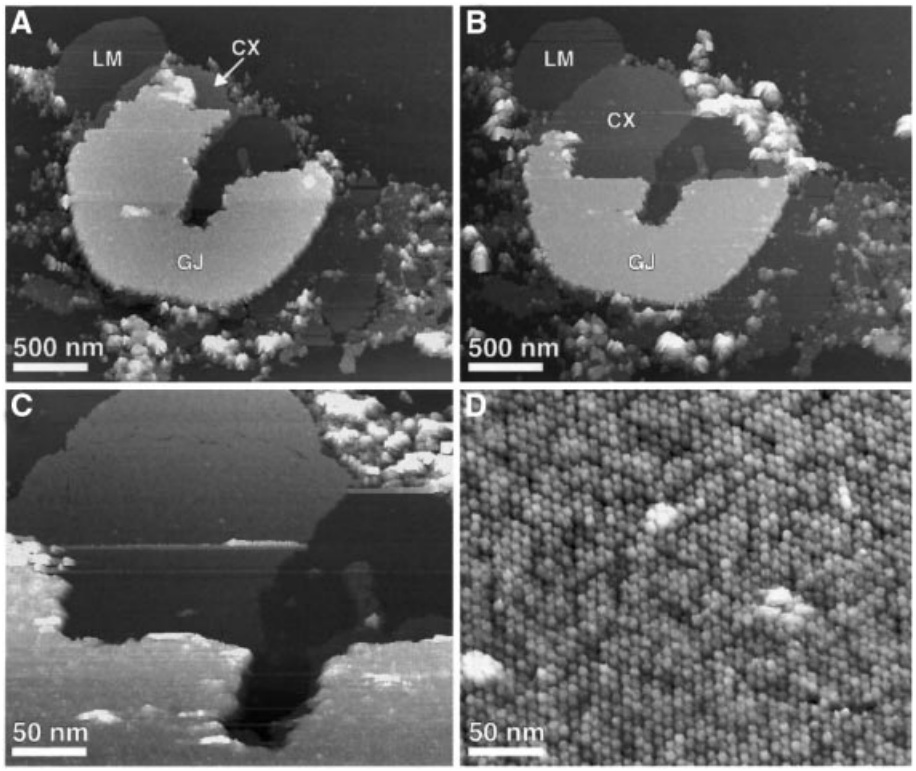

Fig. 1. Gap junction plaque imaged in buffer solution using AFM. (**A**) Overview of a gap junction plaque (marked as GJ) surrounded by a lipid membrane (marked as LM) and fragments of single-layered connexon membranes (marked as CX). (**B**) The same gap junction plaque but partly dissected. The gap junction membrane was dissected by enhancing the applied force from ~50 pN (imaging force) to ~500 pN. After removal, the gap junction plaque was re-imaged at ~50 pN. (**C** and **D**) Extracellular surface of the connexon membrane at elevated magnifications. The hexagonal arrangement of the connexons is clearly visible (D). Topographs were recorded in buffer solution (5 mM Tris, 1 mM EGTA, 1 mM PMSF) with a force of ~50 pN applied to the AFM stylus and a line frequency of 4.4 Hz, and were displayed as relief tilted by 5°. Topographs exhibited a vertical full gray level scale of 25 nm (A–C) and 2.5 nm (D), and were displayed as relief tilted by 5%.

Table I. Summary of pore and thickness sizes measured in AFM images

Morphological feature	Size ± SD (nm) 50 pN imaging force	Size ± SD (nm) 70 pN imaging force
Gap junction bilayer height	4.7 ± 0.6	NA
Non-junctional bilayer height	4.5 ± 0.5	NA
Gap junction height	17.4 ± 0.7	NA
Single connexon layer height	8.0 ± 0.6	NA
Cytoplasmic domain height	1.7 ± 0.2	0.2 ± 0.2
Extracellular domain height	1.6 ± 0.2	NA
Outer diameter of cytoplasmic pore	5.6 ± 0.3	5.8 ± 0.3
Inner diameter of cytoplasmic pore	2.8 ± 0.3	4.7 ± 0.3

NA, not applicable.

Single particle averages of the connexons showed the structural arrangement of the extracellular domains surrounding the transmembrane pore more clearly (Figure 3B). The flexible structural parts of the extracellular connexon surface are indicated in the standard deviation (SD) map (Müller *et al.*, 1998) (Figure 3C). The most flexible region of the extracellular connexon surface was the central pore, exhibiting a SD peak of 0.4 nm, compared with the smallest SD of 0.1 nm, which was detected over the clefts between protruding domains. The lateral resolution of the averages was calculated as ~1.2 nm (see Materials and methods) in Figures 3C and 4C.

Calcium-induced conformational changes in Cx26 hemichannels

A drastic rearrangement of the extracellular connexin domains was observed when imaging the same dissected gap junction plaques in the presence of 0.5 mM Ca^{2+} (Figure 4; Table II). The topograph demonstrates that the channel entrance was significantly smaller, showing a diameter of 0.5 ± 0.3 nm (n = 108) (Figures 4A and B) compared with 1.3 ± 0.3 nm in the absence of Ca^{2+} (Figure 3). There is some slight variability that can seen in the pore sizes of the individual connexons in Figures 3A and 4A. This conformational change was fully reversible

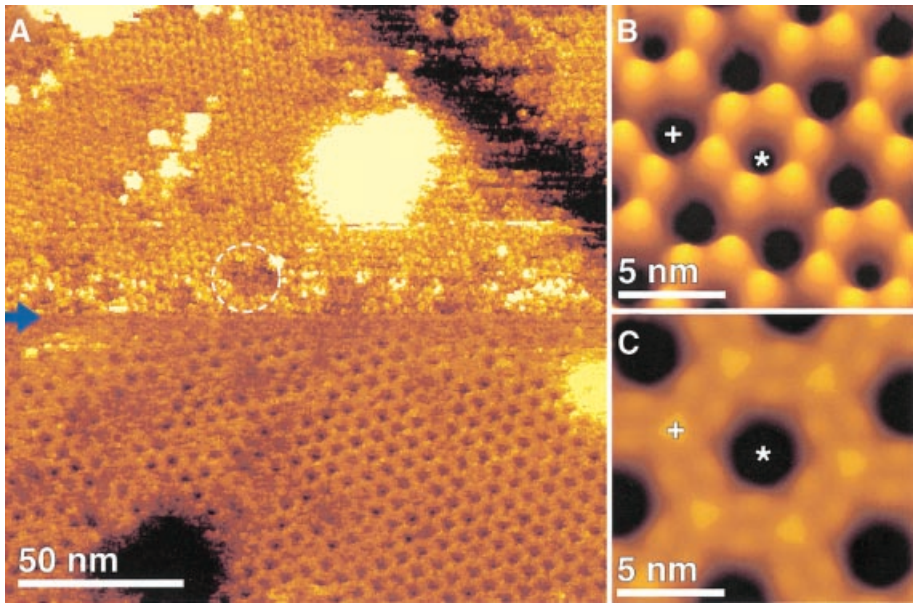

Fig. 2. Two conformations of the cytoplasmic gap junction surface. (**A**) AFM topograph demonstrating the variability of cytoplasmic gap junction domains. Individual gap junction domains appear disordered (circle). The initial applied force of 50 pN (top to center of image) was enhanced at the center of the topograph (blue arrow) to 70 pN (center to bottom of image). A conformational change is distinct: pore forming gap junction hexamers collapse onto the membrane surface, thereby transforming into pores with larger channel diameters. (**B**) Average of the extended conformation of gap junction exhibiting a lateral resolution of ~2 nm. The cytoplasmic domains form a pore (asterisks) and protrude by 1.7 ± 0.2 nm (n = 30) above the lipid bilayer (cross). (**C**) Average of gap junction domains collapsed onto the membrane surface. Here the cytoplasmic domains protrude only by 0.2 ± 0.2 nm (n = 30) above the lipid bilayer (+). Topograph was recorded in Ca^{2+}-free buffer solution (5 mM Tris, 1 mM EGTA and 1 mM PMSF) at a line frequency of 5 Hz. All topographs were displayed as relief tilted by 5°. Topographs exhibit a vertical full gray level scale of 3 nm (A), of 2 nm (B) and of 1 nm (C).

and could be repeated at least five times within 2 h. During such imaging sessions, connexons with intermediate pore sizes between these two states were also observed (data not shown). As indicated by the SD map, the channel entrance, which represented the most flexible structural region of the extracellular connexon surface in the absence of Ca^{2+}, exhibited no significant standard deviation in the presence of Ca^{2+}. This effect indicated an increased stiffness of the extracellular channel entrance induced by the calcium ions. A side-by-side comparison of the correlation averages, as calculated from five independent topographs, showed the hemichannels arranged into a hexagonal lattice (Figure 5A and B). The lateral resolution of these averages was determined as ~1.5 nm (see Materials and methods). The difference image (Figure 5C) calculated between Figure 5A and B, as well as the superposition of contour maps (Figure 5D) between the two conditions, highlights changes in structural features. Figure 5C and D show that the highest difference occurred in the pore area, while the subunit topology exhibited only slight differences.

To be sure that the structural change observed is specific for calcium ions and does not reflect any effect that divalent ions might have on the AFM imaging process (Müller *et al*., 1998) in separate experiments, we added magnesium ions to the imaging buffer. Up to a concentration of 2 mM $MgCl_2$ (instead of Ca^{2+}) did not influence the appearance of the connexon pore.

Calcium-mediated structural change of the gap junction plaque

Calcium-induced conformational changes can also be observed on the cytoplasmic surface of gap junction plaques (Figure 6; Table II). Surprisingly, the gap junction plaque appeared mottled as soon as a minimum of 0.5 mM Ca^{2+} was injected into the buffer solution (Figure 6B). Associated with the mottled appearance, the maximum thickness of the gap junction plaque increased from 17.4 ± 0.7 nm to 18 ± 0.9 nm (n = 33). At higher resolution, the formation of 'islands' was observed on the membrane surface. The maximum height difference of these islands compared with the surrounding deeper regions was 1.5 ± 0.4 nm (n = 23) (Figure 6C). This segregation of material into microdomains within the plaque was associated with an enhanced surface roughness that prevented imaging at submolecular resolution using AFM. Interestingly, it was not possible to reverse this structural change by flushing the AFM fluid cell with a Ca^{2+}-free, EGTA-containing buffer solution.

Discussion

AFM is a powerful tool for imaging the functionality of macromolecules as well as for measuring their dimensions (Drake *et al*., 1989). As the technology continues to develop, AFM is becoming capable of imaging at a higher resolution with the capacity to do physiological imaging on molecular scales under hydrated, ambient conditions (Engel *et al*., 1999; Engel and Müller, 2000). Here we show topographs of Cx26 gap junction samples using AFM in buffer solution at a molecular resolution that is significantly better than has been previously observed (Hoh *et al*., 1991, 1993; Lal *et al*., 1995; Lal and Lin, 2001). The accurate measurements of the morphological features of the intercellular channel and connexon provide

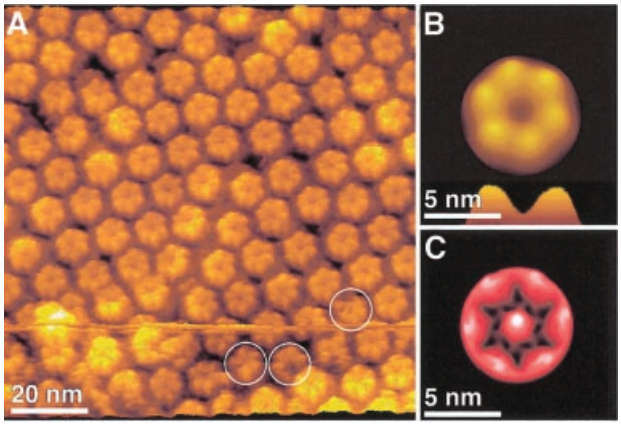

Fig. 3. Extracellular connexon surface recorded in a Ca^{2+}-free buffer solution. (**A**) AFM topograph showing the connexon arrangement. Individual connexons exhibit defects of the size of single connexins as indicated by circles. (**B**) Average of the raw data shown in (A), exhibiting a lateral resolution of ~1.2 nm. Connexin assembly of the connexon and the extracellular channel opening (profile at bottom) are clearly seen. (**C**) To access the flexibility of the structural details, a SD map of the average was calculated (Müller *et al*., 1998). The SD map had a range from 0.1 nm (black) to 0.4 nm (white), and is shown in black to red to white shades. The maximum SD value located at the connexon pore indicates an enhanced structural variability of this area. The topograph was recorded in buffer solution (5 mM Tris, 1 mM EGTA and 1 mM PMSF) at an applied force of 50 pN and a line frequency of 5.5 Hz, and has a vertical scale of 2 nm. All images were displayed as relief tilted by 5°.

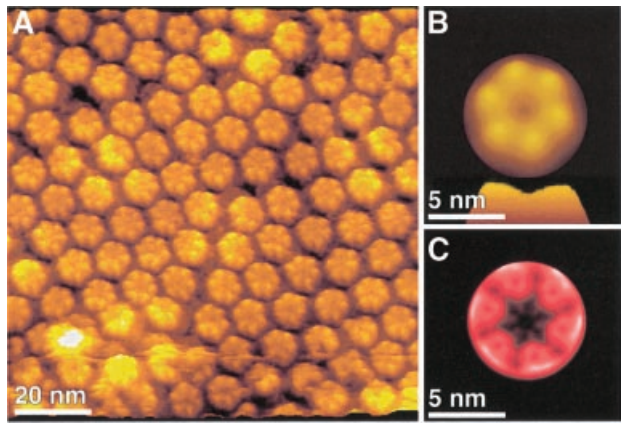

Fig. 4. Ca^{2+}-induced conformational change of the extracellular connexon surface. (**A**) Same connexon surface as imaged in Figure 3, but in the presence of 0.5 mM $CaCl_2$. As visible in the raw data, individual connexons nearly closed their channel entrance. The average, exhibiting a lateral resolution of ~1.2 nm (**B**), shows details of this structural change more clearly. The channel has changed significantly (profile at bottom of figure). Superposition of correlation average and SD map (**C**) allows assigning the channel entrance to be the most rigid structural element of the extracellular surface. The topograph was recorded in buffer solution (5 mM Tris, 0.5 mM $CaCl_2$ and 1 mM PMSF) at an applied force of 50 pN and a line frequency of 5.5 Hz. While the topographs had a vertical range of 2 nm, the SD map extended from 0.1 to 0.3 nm. All images were displayed as relief tilted by 5°.

a basis for computer modeling of gating. In addition, if regulators can be found that mimic the native physiological state in which most channels in the plaque are docked but only a few are actually open (Bukauskas *et al*., 2000), then AFM will be an excellent tool for discriminating between these channel types.

Comparison of the overall thickness of Cx26 gap junctions with other gap junction preparations

Since the *z*-modulation in AFM images is very well determined (Binnig *et al*., 1986; Drake *et al*., 1989), thickness measurements of biological specimens can be made to within a few Å (Müller and Engel, 1997). In addition, topographs recorded by AFM provide accurate measurements for the dimensions of molecular features, such as pore dimensions and the height of the cytoplasmic and extracellular domains protruding from the lipid bilayer. Estimates of these features have been achieved using small angle X-ray diffraction (Makowski *et al*., 1977; Unwin and Ennis, 1983) and electron crystallography (Unwin and Ennis, 1984; Unger *et al*., 1999) of mouse and rat liver gap junctions that contained mixtures of connexin isoforms. While small angle X-ray diffraction gives thicknesses to a high degree of precision (Makowski *et al*., 1977), in EM reconstructions the lipid bilayers often appear invisible due to limited resolution and contrast and therefore, transmembrane domain boundaries can only be estimated. Alternatively, EM investigations of thin sections give an approximate value to within ~1 nm. We determined the thickness of gap junction plaques to be 17.4 ± 0.7 nm, which is in good agreement with the gap junction thickness of 17.0 ± 0.5 nm (n = 55) from thin sections of pelleted Cx26 gap junctions. Cx32 gap junctions from rat liver and Cx43 from cardiac tissue showed thicknesses of ~18 nm (Sosinsky *et al*., 1988) and ~25 nm (Yeager, 1998), respectively. The 0.7 nm electron crystallographic structure of a gap junction (Unger *et al*., 1999) shows primarily the transmembrane and extracellular domains, which constitute a thickness of ~15 nm. The C-terminal ends of these connexons show a net difference of ~58 amino acids (aa) between Cx26 and Cx32, and a difference of ~139 aa between Cx26 and Cx43. Cx26, which exhibits the shortest C-terminal end in the connexin family (Zhang and Nicholson, 1994), shows a minimum thickness. The thickness of the other Cx forms increases with the length of their C-terminal end. Thus, the difference in height compared with other connexons is most likely due to the difference in size of the C-terminal tail.

Conformations of the cytoplasmic surface

The high-resolution topographs of the gap junction surface (Figure 2) represent the first structural data resolving individual cytoplasmic connexin domains. In previous 3D reconstructions from EM, it was not possible to visualize these domains (Unwin and Ennis, 1984; Perkins *et al*., 1997; Unger *et al*., 1999). It has been speculated that the connexon structure at the cytoplasmic surface is crystallographically disordered, particularly in low resolution (>15 Å) structures (Sosinsky *et al*., 1988; Sosinsky, 1992; Perkins *et al*., 1997). The higher resolution structure of a truncation mutant of Cx43 (263 total aa; Unger *et al*., 1999) containing a longer C-terminus than Cx26 (226 total aa), shows some cytoplasmic surface structure. However, since these cytoplasmic segments were crystallographically disordered in the EM preparations investigated, the averaged surface structures were short and unconnected. EM images of thin sections of tannic acid-fixed rat liver

gap junctions contained wispy protein extensions at the cytoplasmic surface (Sosinsky *et al*., 1988). This observation is in apparent contrast to our finding that the C-terminal domains can co-exist in a structurally ordered conformation. It may be concluded that the cytoplasmic domains observed in our experiments may not be sufficiently crystallographically ordered in preparations that are studied by EM. These results suggest that the specimen conditions are crucial in maintaining the native conformation of the cytoplasmic gap junction domains.

The AFM topographs presented here provide a surface view of the structure, and show that the native cytoplasmic gap junction domains are indeed flexible but that these domains can rearrange into an ordered structure. The unperturbed structure of the domains extended by 1.7 ± 0.2 nm into the aqueous space and formed a hexameric pore exhibiting a channel diameter (2.8 nm; Figure 2A) at the cytoplasmic opening. In contrast, the observed channel diameter at the height of the lipid bilayer surface was found to be much broader (4.7 nm; Figure 2B), suggesting that the cytoplasmic channel exhibits significantly different diameters.

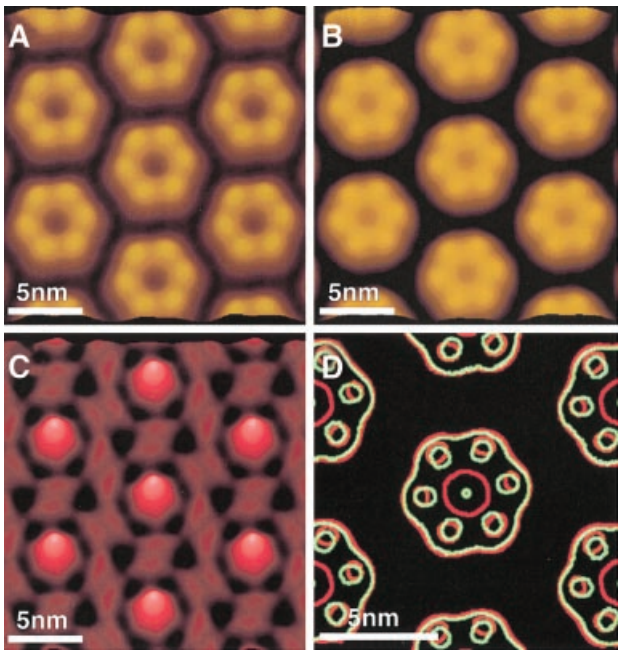

Fig. 5. Connexon surface as a function of Ca^{2+} concentration. Extracellular surfaces of connexons displayed in an idealized 2D lattice were recorded in the absence (**A**) and presence (**B**) of Ca^{2+}. Correlation averages shown were calculated from several topographs recorded under equivalent conditions. The lateral resolution of the averages was limited to ~1.5 nm. To visualize their differences, a difference map was calculated (**C**). (**D**) Superimposed contours of the two conformations (red, no Ca^{2+}; green, with Ca^{2+}). All presentations show that the most significant change is observed at the pore. The contour plots, however, show that in the presence of Ca^{2+} the connexin surface protrusions move towards the pore center. Note that the greatest difference is in the size of the pore. The images exhibiting a vertical gray level range of 2 nm (A and B) and 0.8 nm (C) were displayed as relief tilted by 5°.

Force and energy required to alter the conformation of cytoplasmic domains

The flexible cytoplasmic domains were reversibly rearranged by the AFM stylus after slightly increasing the imaging forces from 50 to 70 pN. The energy difference (ΔE) forcing the domains into a different conformation was 3.4 kJ/mol, which resulted from the force difference of 20 pN and a height reduction of 1.7 nm. In contrast, the total energy (E) of 11.9 kJ/mol (resulting from the applied force of 70 pN and resulting in a height reduction of 1.7 nm), distorting the structural arrangement of the cytoplasmic domains, was between four and five times higher than the *k*T at room temperature (2.5 kJ/mol). Such a low value is compatible with the reversibility of the process. It also implies that the extended C-terminal end was only meta-stable, explaining its molecular disorder by changing the experimental procedure as observed by EM. This inherent structural flexibility, particularly in the C-terminus, forms the basis of the particle-receptor hypothesis for Cx43 proposed by Delmar and co-workers (Delmar *et al*., 2000). It should be noted that although Cx26 has a small C-terminus and this model of 'particle' gating may not apply to this isoform, the flexibility is probably still an important feature intrinsic to all connexins.

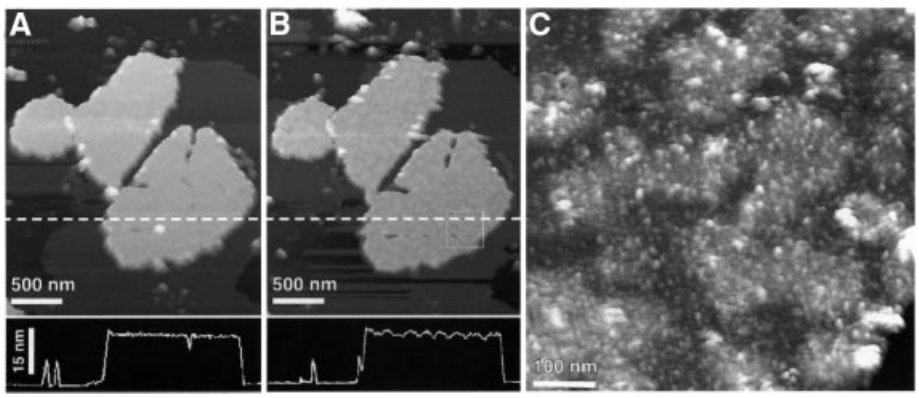

Fig. 6. Ca^{2+}-induced conformational change of the gap junction plaque. (**A**) The topograph was recorded in buffer solution (5 mM Tris and 1 mM PMSF) using contact mode AFM at an applied force of 50 pN and a line frequency of 4 Hz. (**B**) The same gap junction plaque after injection of 0.5 mM Ca^{2+} into the buffer solution. The gap junction surface formed islands of variable heights and the height of the plaque increased to 18 ± 0.9 nm (n = 33), by ~0.6 nm. At higher magnification (**C**), an enhanced roughness of the buckled surface was observed. All topographs were recorded at an applied force of 50 pN and a line frequency between 4 and 5 Hz. The images exhibiting a vertical gray level range of 25 nm (A and B) and 5 nm (C) were displayed as relief tilted by 5°.

Relation to other inter- and intramolecular forces

The force of 70 pN required to induce the putative compression of the connexin C-terminal end is remarkably close to the 100–150 pN reported to produce a conformational change of individual polypeptide loops connecting two transmembrane α-helices E and F of bacteriorhodopsin (Müller *et al*., 1995, 1999b). However, the C-terminal end of Cx26 is more than seven times larger compared to of the polypeptide loop (8 aa) of bacteriorhodopsin. Thus, the inherent flexibility makes the connexin C-terminal end acutely sensitive to perturbations by the AFM probe. Interestingly, binding forces between avidin and biotin (160 pN; Florin *et al*., 1994), streptavidin and biotin (340 pN; Lee *et al*., 1994), antigen and antibody complexes (60 pN; Dammer *et al*., 1996), and unfolding of transmembrane α-helices (100–200 pN; Oesterhelt *et al*., 2000) are within the same range as the force applied to induce the conformational change in the cytoplasmic Cx26 domain. Note that forces for stripping the top connexon layer off (⩾500 pN) are approximately one order of magnitude higher, indicative of the strong hydrophobic forces holding the two extracellular connexon surfaces together (Ghoshroy *et al*., 1995). At present, the force-induced conformational change of the cytoplasmic surface does not permit a discrimination of the two postulated mechanisms, compression (i.e. a tertiary structural rearrangement) or a vertical displacement (i.e. a breakage of specific short-range weak molecular interactions within the connexon).

Structural comparisons

Using cryo-EM, Unger *et al*. (1999) found the cytoplasmic pore of the Cx43 truncation mutant to exhibit an inner diameter of 4 nm at the lipid bilayer surface. This value fits well with the 4.7 nm measured at applied forces of 70 pN (Figure 2C). A 3D reconstruction of a negatively stained rat liver gap junction, which primarily contains Cx32 (Cx32:Cx26 in a ratio of 10:1), showed a diameter of 2.5 nm at the cytoplasmic end of the channel (Perkins *et al*., 1997). Again, this value agrees well with the inner channel diameter (2.8 nm) detected on fully extended cytoplasmic domains (Figure 2B).

Extracellular surface structure

After dissection of the junctional plaque, the extracellular connexon surface was observed. The individual domains formed a hexameric pore exhibiting an outer diameter of 4.9 ± 0.3 nm and protruding by 1.6 ± 0.2 nm from the lipid bilayer. The channel of the pore, however, had an inner channel diameter of 1.5 ± 0.3 nm, which was significantly smaller than that observed for the cytoplasmic pore. Using cryo-EM, Unger *et al*. (1999) found the opening of the extracellular Cx43 pore to have an outer diameter of 5 nm and an inner diameter of 2.5 nm. These observations agree reasonably well with our structural data, although the connexons investigated originated from different isoforms confirming conserved structural topology among connexins.

Considering the structural data together, both connexon surfaces reveal a channel diameter of ~2.8 nm (FWHM) at the cytoplasmic end, which expands to ~4.7 nm at the cytoplasmic lipid bilayer surface. Towards the extracellular end, this channel is then tapered to ~1.5 nm.

Calcium-induced conformational changes in connexons and gap junction plaque

While there are other effectors, such as pH, that open and close the channels, calcium ions have long been postulated to play a crucial role in the gating of the gap junction intercellular channel. Uncoupling can be a protective mechanism for cells to isolate themselves from harmful ionic concentrations as well as in normal cellular functions (Peracchia *et al*., 1994). In a mammalian cell system, Lazrak and Peracchia (1993) showed that Cx43 channels are sensitive to Ca^{2+} ions in concentrations as low as in the nanomolar range, but are insensitive to pH in the range of 6.1–7.2 (Lazrak and Peracchia, 1993). Recent studies have shown that hemichannels in the plasma membrane are also sensitive to Ca^{2+} ions in mM concentrations similar to those used in this study (Li *et al*., 1996; Pfahnl and Dahl, 1999) as opposed to the submicromolar concentrations of Ca^{2+} ions found inside the cell cytoplasm (Lazrak and Peracchia, 1993). This differing sensitivity would allow for closing of a gate at the extracellular end of hemichannels that preserves the homeostatic mixture of cytoplasmic components, while the higher sensitivity of a gate at the cytoplasmic surface would accommodate situations where high levels of Ca^{2+} ions signal cell injury or death. In addition, *in vivo* studies of hemichannels have shown a slow response time (seconds to minutes) to Ca^{2+} ions in millimolar concentrations rather than a fast response time (milliseconds or less) for the cytoplasmic gate, which is consistent with our observations of this *in vitro* system. Trexler *et al*. (1996) postulated a 'loop gate' in isolated hemichannels and a cytoplasmic 'cell–cell channel' gating mechanism for paired, docked connexons.

In our experiments, adding Ca^{2+} to the buffer solution resulted in a conformational change in the extracellular connexon pores when we examined single connexon layers. This closure was specific to Ca^{2+} because Mg^{2+} in similar concentrations showed no effect. Individual connexons changed their channel diameter from 1.5 to

Table II. Comparison of features in the absence (–Ca^{2+}) and presence (+Ca^{2+}) of Ca^{2+}

Morphological feature	–Ca^{2+} Size ± SD (nm)	+Ca^{2+} Size ± SD (nm)
Outer diameter of extracellular pore	4.9 ± 0.3	4.8 ± 0.3
Inner diameter of extracellular pore	1.3 ± 0.3	0.5 ± 0.3
Gap junction height	17.4 ± 0.7	18 ± 0.9
Modulation of cytoplasmic microdomains	NA	1.5 ± 0.4

NA, not applicable.

0.6 nm (Figures 3 and 4). With the accuracy of our measurements, we did not observe a height change at the extracellular surface of the connexons associated with the conformational change. Furthermore, we did not observe a rotation of the extracellular domains as shown in Figure 5. The absence of connexin rotation at the extracellular surface is in good agreement with the findings of Unwin and Ennis (1984). When analyzing EM data of Ca^{2+}-exposed connexons, it was observed that the cytoplasmic but not the extracellular connexin domains rotate, thereby closing the connexon channel. The observation, however, that this conformational change affects the extracellular connexon surface is new and we hypothesize that we are observing a different gating mechanism for hemichannels. Based on the responses to calcium ions demonstrated here, we also speculate that previously docked connexons can relax back to a hemichannel conformation once separated from their partner connexons. Since no 3D structure exists for pre-docked or undocked connexons, it has not been demonstrated whether the extracellular surface conformation in undocked and previously docked channels differs or is the same. Previous work by Perkins *et al*. (1998) showed that at ~16 Å resolution, the surfaces were still sufficiently maintained in previously docked connexons so that the valleys of one connexon almost perfectly matched the peaks of the extracellular surfaces of its partner connexon. In addition, the computationally docked dodecamers fit well into independently obtained 3D structures of intact gap junction channels.

Intact gap junction plaques containing paired docked connexons exposed to Ca^{2+} showed an unusual structural reaction. The cytoplasmic surface of the entire plaque changed its appearance, forming islands of different heights (Figure 6). Compared with Ca^{2+}-free experiments, the maximum height of the Ca^{2+} exposed gap junctions increased slightly by 0.6 nm to 18 nm. This height increase of 3.3% is close to the 4% detected by low angle X-ray analysis (Unwin and Ennis, 1983). However, the height increase of the gap junction plaque observed here is not homogeneous. The segregation of the gap junction plaque into distinguishable islands suggests an alternative interpretation, whereby conformational changes at the extracellular surface upon Ca^{2+} exposure change the packing within the plaque. Peracchia (1978) observed, using freeze fracture of lens fiber gap junctions, that isolated gap junctions containing low Ca^{2+} concentrations ($>10^{-7}$ M) contained tightly and regularly packed gap membrane particles (channels). Gap junctions isolated in bicarbonate–EDTA buffers had loosely and irregularly arranged membrane channels, indicating a reordering of the membrane channels due to calcium ions. An alternative interpretation is that the formation of islands is due to protein denaturation due to this high level of calcium ions. The structural change we observed may also influence the interaction between connexons of apposing membranes and the interaction between connexons within a membrane leaflet. As a consequence, the docking between two connexons may not function satisfactorily, thereby affecting the connexon–connexon interaction at the extracellular surface (Perkins *et al*., 1998). It has recently been observed that such intermolecular interactions demonstrate the potential to reversibly stimulate the assembly of membrane proteins into crystalline arrays (Möller *et al*., 2000).

Conclusions

Gap junctions play important roles in maintaining intercellular communication. The connexons forming the communication channels between two adjacent cells must react to environmental and intracellular stimuli. It has been shown previously that in intact cells, Ca^{2+} stimulates the gap junctions to close the intercellular channel at submicromolar amounts, and hemichannels at millimolar concentrations. Here, it was observed that in the presence of Ca^{2+}, the extracellular connexon pore reduces its channel diameter significantly in hemichannels. In what may be a different phenomenon, the gap junction plaques change appearance with the presence of Ca^{2+}, possibly related to a conformational change in the intact connexin channel or a lattice rearrangement of channels. The flexibility of the C-terminal end has been postulated to relate to the function of the cytoplasmic domains being involved in the potential dependent gating of gap junctions. These hypotheses remain to be proven in future experiments.

Materials and methods

Atomic force microscopy

Instrumentation. After the biological specimen was adsorbed to mica (Müller *et al*., 1997), the sample was mounted on the piezoelectric scanner of the atomic force microscope (Nanoscope III; Digital Instruments, Santa Barbara, CA) equipped with a liquid cell. The piezoelectric scanner had a scan range of 100×100 μm^2 and was calibrated as described previously (Müller and Engel, 1997). Cantilevers had nominal force constants of k = 0.09 N/m and oxide-sharpened Si_3N_4 probes (Olympus Ltd, Tokyo, Japan). After thermal relaxation, the drift of the cantilever deflection angle was at a minimum. Initial engagement of the probe was performed by setting the scan size at zero to minimize specimen deformation or probe contamination. Prior to scanning the sample, the operating point of the microscope was set to forces below 0.2 nN.

AFM imaging. Unless stated differently, all topographs were recorded using the constant force mode at an applied force of ~50 pN. At low magnification (frame size >600 nm at 512×512 pixels), images were recorded in the error signal mode (Putman *et al*., 1992), acquiring the deflection and height signals simultaneously. The deflection signal was minimized, adjusting gains and scan speed. The scan speed was roughly linear to the scan size, 4–8 lines per second for lower magnifications (frame sizes 13 to 0.5 μm) and 10–17 lines per second for higher magnifications (frame sizes 130 to 80 nm). All measurements were performed in buffer solution (see figure legends) under ambient pressure and at room temperature (21°C). Force dissection procedures followed those of Hoh *et al*. (1991, 1993) using forces ⩾500 pN.

Calcium experiments

After imaging the sample in 5 mM Tris and 1 mM phenyl methylsulfonylfluoride (PMSF), the buffer solution of the AFM liquid cell was exchanged with 5 mM Tris, 0.5 mM $CaCl_2$ and 1 mM PMSF. After a relaxation time of ~5–15 min, the sample was re-imaged using the same imaging parameters without exchange of the AFM stylus. Removal of $CaCl_2$ was performed by exchanging the buffer solution of the AFM liquid cell with 5 mM Tris, 1 mM EGTA and 1 mM PMSF (experiments not shown).

Image processing and averaging

Topographs (512×512 pixels) were selected by the quality of the structural details imaged reproducibly and by comparing the simultaneously monitored height profiles acquired in trace and retrace direction. For image processing, the raw data were transferred to an ALPHA workstation and analyzed using the SEMPER image processing system (Saxton *et al*., 1979). For correlation averaging, a well preserved unit cell was selected from the raw data and cross-correlated with the topograph (Saxton and Baumeister, 1982). For the connexons shown in Figure 5, correlation peaks identified the unit cell positions within the two-

dimensional (2D) crystal and allowed lattice distortions to be unbent by fitting spline functions through the peaks and re-sampling the topograph along optimized coordinates (Saxton *et al*., 1992). Single particle averages were also generated by extracting unit cells according to the peak coordinates, translationally and rotationally aligning them to a reference connexon and then averaging them (Figures 3B and 4B). The resulting correlation average was used as reference for refinement cycles (Saxton *et al*., 1984). Correlation averaged unit cells were either 3- or 6-fold symmetrized. The lateral resolution of the averages was estimated according to the Fourier ring correlation function (Saxton and Baumeister, 1982), the phase residual (Frank and Boublik, 1981), and the spectral signal-to-noise ratio (Unser *et al*., 1987). To assess the standard deviation, $\sigma_{k,l}$ individual unit cells were extracted according to the coordinates of their correlation peaks and were aligned angularly as well as translationally before single particle averaging (Frank *et al*., 1988). The standard deviation was then calculated from the averaged topograph $\mu_{k,l}$ for each pixel (k, l) for x^i particles (Schabert and Engel, 1994):

$$\sigma^2_{k,l} = \frac{1}{N}\sum_{i-1}^{N}(x^i_{k,l} - \mu_{k,l})^2$$

These standard deviations were displayed as an image (Figures 3C and 4C) in a one-to-one pixel correspondence with the original images. The values range from 0.1 nm (black) to 0.4 nm (white), with the colour table continuously ranging from black to red to white shades.

Preparation of Cx26 gap junction plaques

Gap junction purification follows the procedure described in detail in Hand *et al*. (2001). Briefly, an overexpressing Cx26 HeLa cell line was grown to confluence. The cells were collected and sonicated to lyse them. A plasma membrane fraction was purified using a discontinuous sucrose gradient and then treated sequentially with sarkosyl, Brij 58 and saponin. After detergent treatments, the gap junction fraction was collected at the 30%/41% interface of a second discontinuous gradient. The interface fraction is diluted with Tris–EGTA buffer and pelleted at ~86 000 *g* for 30 min. The pellet is resuspended with buffer and recentrifuged to eliminate the sucrose solution. Finally, the pellet containing the purified gap junctions was resuspended in a 5 mM Tris, 1 mM EGTA buffer containing 0.02% sodium azide and 1 mM PMSF.

Acknowledgements

This work was supported by the Maurice E.Müller Foundation and the Swiss National Funds (grant no. 4036-44062) awarded to A.E. and the National Science Foundation (grant no. MCB-9728338 and MCB-0131425) awarded to G.S. Some of the work included here was conducted at the National Center for Microscopy and Imaging Research at San Diego, which is supported by National Institutes of Health grant no. RR04050 awarded to Dr Mark Ellisman.

References

Binnig,G., Quate,C.F. and Gerber,C. (1986) Atomic force microscope. *Phys. Rev. Lett.*, **56**, 930–933.

Bukauskas,F.F., Jordan,K., Bukauskiene,A., Bennett,M.V., Lampe,P.D., Laird,D.W. and Verselis,V.K. (2000) Clustering of connexin 43-enhanced green fluorescent protein gap junction channels and functional coupling in living cells. *Proc. Natl Acad. Sci. USA*, **97**, 2556–2561.

Czajkowsky,D.M. and Shao,Z. (1998) Submolecular resolution of single macromolecules with atomic force microscopy. *FEBS Lett.*, **430**, 51–54.

Dammer,U., Hegner,M., Anselmetti,D., Wagner,P., Dreier,M., Huber,W. and Güntherodt,H.J. (1996) Specific antigen/antibody interactions measured by force microscopy. *Biophys. J.*, **70**, 2437–2441.

Delmar,M., Stergiopoulos,K., Homma,N., Calero,G., Morley,G., Ek-Vitorin,J.F. and Taffet,S.M. (2000) A molecular model for the chemical regulation of connexin43 channels: the 'ball and chain' hypothesis in gap junctions. In Peracchia,C. (ed.), *Molecular Basis of Cell Communication in Health and Disease*. Academic Press, San Diego, CA, pp. 223–248.

DeMello,W.C. (1975) Effects of intracellular injection of calcium and strontium on cell communication in heart. *J. Physiol.*, **250**, 231–245.

Drake,B., Prater,C.B., Weisenhorn,A.L., Gould,S.A.C., Albrecht,T.R., Quate,C.F., Cannell,D.S., Hansma,H.G. and Hansma,P.K. (1989) Imaging crystals, polymers and processes in water with the atomic force microscope. *Science*, **243**, 1586–1588.

Engel,A. and Müller,D.J. (2000) Observing single biomolecules at work with the atomic force microscope. *Nat. Struct. Biol.*, **7**, 715–718.

Engel,A., Schoenenberger,C.-A. and Müller,D.J. (1997) High-resolution imaging of native biological sample surfaces using scanning probe microscopy. *Curr. Opin. Struct. Biol.*, **7**, 279–284.

Engel,A., Lyubchenko,Y. and Müller,D.J. (1999) Atomic force microscopy: a powerful tool to observe biomolecules at work. *Trends Cell Biol.*, **9**, 77–80.

Florin,E.-L., Moy,V.T. and Gaub,H.E. (1994) Adhesion forces between individual ligand-receptor pairs. *Science*, **264**, 415–417.

Fotiadis,D., Müller,D.J., Tsiotis,G., Hasler,L., Tittmann,P., Mini,T., Jenö,P., Gross,H. and Engel,A. (1998) Surface analysis of the photosystem I complex by electron and atomic force microscopy. *J. Mol. Biol.*, **283**, 83–94.

Fotiadis,D., Hasler,L., Müller,D.J., Stahlberg,H., Kistler,J. and Engel,A. (2000) Surface tongue-and-groove contours on lens MIP facilitate cell-to-cell adherence. *J. Mol. Biol.*, **300**, 779–789.

Fotiadis,D., Scheuring,S., Müller,S., Engel,A. and Müller,D.J. (2002) Controlled nanomanipulation of biological specimens with the atomic force microscope. *Micron*, **33**, 385–397.

Frank,J. and Boublik,M. (1981) Computer averaging of electron micrographs of 40S ribosomal subunits. *Science*, **214**, 1353–1355.

Frank,J., Bretaudiere,J.-P., Carazo,J.-M., Veschoor,A. and Wagenknecht,T. (1988) Classification of images of biomolecular assemblies: a study of ribosomes and ribosomal subunits of *Escherichia coli*. *J. Microsc.*, **150**, 99–115.

Ghoshroy,S., Goodenough,D.A. and Sosinsky,G.E. (1995) Preparation, characterization and structure of half gap junctional layers split with urea and EGTA. *J. Membr. Biol.*, **146**, 15–28.

Hand,G.M., Müller,D.J., Nicholson,B., Engel,A. and Sosinsky,G.E. (2002) Isolation and characterization of gap junctions from tissue culture cells. *J. Mol. Biol.*, **315**, 587–600.

Hoh,J.H., Lal,R., John,S.A., Revel,J.-P. and Arnsdorf,M.F. (1991) Atomic force microscopy and dissection of gap junctions. *Science*, **253**, 1405–1408.

Hoh,J.H., Sosinsky,G.E., Revel,J.-P. and Hansma,P.K. (1993) Structure of the extracellular surface of the gap junction by atomic force microscopy. *Biophys. J.*, **65**, 149–163.

Kamermans,M., Fahrenfort,I., Schultz,K., Janssen-Bienhold,U., Sjoerdsma,T. and Weiler,R. (2001) Hemichannel-mediated inhibition in the outer retina. *Science*, **292**, 1178–1180.

Lal,R. and Lin,H. (2001) Imaging molecular structure and physiological function of gap junctions and hemijunctions by multimodal atomic force microscopy. *Microsc. Res. Tech.*, **52**, 273–288.

Lal,R., John,S.A., Laird,D.W. and Arnsdorf,M.F. (1995) Heart gap junction preparations reveal hemiplaques by atomic force microscopy. *Am. J. Physiol. Cell Physiol.*, **37**, C968–C977.

Lazrak,A. and Peracchia,C. (1993) Gap junction gating sensitivity to physiological internal calcium regardless of pH in Novikoff hepatoma cells. *Biophys. J.*, **65**, 2002–2012.

Lee,G.U., Kidwell,D.A. and Colton,R.J. (1994) Sensing discrete streptavidin–biotin interactions with atomic force microscopy. *Langmuir*, **10**, 354–357.

Li,H., Liu,T.-F., Lazrak,A., Peracchia,C., Goldberg,G.S., Lampe,P.D. and Johnson,R.G. (1996) Properties and regulation of gap junctional hemichannels in the plasma membrane of cultured cells. *J. Cell Biol.*, **134**, 1019–1030.

Loewenstein,W.R. (1966) Permeability of membrane junctions. *Ann. NY Acad. Sci.*, **137**, 441–472.

Loewenstein,W.R., Nakas,M. and Socolar,S.J. (1967) Junctional membrane uncoupling. Permeability transformation at a cell membrane junction. *J. Gen. Physiol.*, **50**, 1865–1891.

Makowski,L., Caspar,D.L.D., Phillips,W.C. and Goodenough,D.A. (1977) Gap junction structure II. Analysis of the X-ray diffraction data. *J. Cell Biol.*, **74**, 629–645.

Möller,C., Büldt,G., Dencher,N., Engel,A. and Müller,D.J. (2000) Reversible loss of crystallinity on photobleaching purple membrane in presence of hydroxylamine. *J. Mol. Biol.*, **301**, 869–879.

Müller,D.J. and Engel,A. (1997) The height of biomolecules measured with the atomic force microscope depends on electrostatic interactions. *Biophys. J.*, **73**, 1633–1644.

Müller,D.J., Büldt,G. and Engel,A. (1995) Force-induced conformational change of bacteriorhodopsin. *J. Mol. Biol.*, **249**, 239–243.

Müller,D.J., Amrein,M. and Engel,A. (1997) Adsorption of biological molecules to a solid support for scanning probe microscopy. *J. Struct. Biol.*, **119**, 172–188.

Müller,D.J., Fotiadis,D. and Engel,A. (1998) Mapping flexible protein domains at subnanometer resolution with the AFM. *FEBS Lett.*, **430**, 105–111.

Müller,D.J., Fotiadis,D., Scheuring,S., Müller,S.A. and Engel,A. (1999a) Electrostatically balanced subnanometer imaging of biological specimens by atomic force microscopy. *Biophys. J.*, **76**, 1101–1111.

Müller,D.J., Sass,H.-J., Müller,S., Büldt,G. and Engel,A. (1999b) Surface structures of native bacteriorhodopsin depend on the molecular packing arrangement in the membrane. *J. Mol. Biol.*, **285**, 1903–1909.

Oesterhelt,F., Oesterhelt,D., Pfeiffer,M., Engel,A., Gaub,H.E. and Müller,D.J. (2000) Unfolding pathways of individual bacteriorhodopsins. *Science*, **288**, 143–146.

Oliveira-Castro,G.M. and Loewenstein,W.R. (1971) Junctional membrane permeability: Effects of divalent cations. *J. Membr. Biol.*, **5**, 51–77.

Peracchia,C. (1978) Calcium effects on gap junction structure and cell coupling. *Nature*. **271**, 669–671.

Peracchia,C., Lazrak,A. and Peracchia,L.L. (1994) Molecular models of channel interaction and gating in gap junctions. In Peracchia,C. (ed.), *Membrane Channels*. Academic Press, New York, NY, pp. 361–377.

Perkins,G.A., Goodenough,D. and Sosinsky,G. (1997) Three-dimensional structure of the gap junction connexon. *Biophys. J.*, **72**, 533–544.

Perkins,G.A., Goodenough,D.A. and Sosinsky,G.E. (1998) Formation of the gap junction intercellular channel requires a 30° rotation for interdigitating two apposing connexons. *J. Mol. Biol.*, **277**, 171–177.

Pfahnl,A. and Dahl,G. (1999) Gating of cx46 gap junction hemichannels by calcium and voltage. *Pflugers Arch.*, **437**, 345–353.

Putman,C.A.J., van der Werft,K., de Grooth,B.G., van Hulst,N.F., Greve,J. and Hansma,P.K. (1992) A new imaging mode in the atomic force microscopy based on the error signal. *SPIE*, **1639**, 198–204.

Rottingen,J. and Iversen,J.G. (2000) Ruled by waves? Intracellular and intercellular calcium signalling. *Acta Physiol. Scand.*, **169**, 203–219.

Saxton,W.O. and Baumeister,W. (1982) The correlation averaging of a regularly arranged bacterial cell envelope protein. *J. Microsc.*, **127**, 127–138.

Saxton,W.O., Pitt,T.J. and Horner,M. (1979) Digital image processing: the semper system. *Ultramicroscopy*, **4**, 343–354.

Saxton,W.O., Baumeister,W. and Hahn,M. (1984) Three-dimensional reconstruction of imperfect two-dimensional crystals. *Ultramicroscopy*, **13**, 57–70.

Saxton,W.O., Dürr,R. and Baumeister,W. (1992) From lattice distortion to molecular distortion: characterising and exploiting crystal deformation. *Ultramicroscopy*, **46**, 287–306.

Schabert,F.A. and Engel,A. (1994) Reproducible acquisition of *Escherichia coli* porin surface topographs by atomic force microscopy. *Biophys. J.*, **67**, 2394–2403.

Schabert,F.A., Henn,C. and Engel,A. (1995) Native *Escherichia coli* OmpF porin surfaces probed by atomic force microscopy. *Science*, **268**, 92–94.

Schwarz,U.D., Haefke,H., Reimann,P. and Guntherodt,H.J. (1994) Tip artefacts in scanning force microscopy. *J. Microsc.*, **173**, 183–197.

Sosinsky,G.E. (1992) Image analysis of gap junction structures. *Electron Microsc. Rev.*, **5**, 59–76.

Sosinsky,G.E., Jesior,J.C., Caspar,D.L. and Goodenough,D.A. (1988) Gap junction structures. VIII. Membrane cross-sections. *Biophys. J.*, **53**, 709–722.

Trexler,E.B., Bennett,M.V.L., Bargiello,T.A. and Verselis,V.K. (1996) Voltage gating and permeation in a gap junction hemichannel. *Proc. Natl Acad. Sci. USA*, **93**, 5836–5841.

Unger,V.M., Kumar,N.M., Gilula,N.B. and Yeager,M. (1999) Three-dimensional structure of a recombinant gap junction membrane channel. *Science*, **283**, 1176–1180.

Unser,M., Trus,B.L. and Steven,A.C. (1987) A new resolution criterion based on spectral signal-to-noise ratios. *Ultramicroscopy*, **23**, 39–52.

Unwin,P.N.T. and Ennis,P.D. (1983) Calcium-mediated changes in gap junction structure: evidence from the low angle X-ray pattern. *J. Cell Biol.*, **97**, 1459–1466.

Unwin,P.N.T. and Ennis,P.D. (1984) Two conformations of a channel-forming membrane protein. *Nature*, **307**, 609–613.

Unwin,P.N.T. and Zampighi,G. (1980) Structure of the junction between communicating cells. *Nature*, **283**, 545–548.

Willecke,K., Eiberger,J., Degen,J., Eckardt,D., Romualdi,A., Güldenagel,M., Deutsch,U. and Söhl,G. (2002) Structural and functional diversity of connexin genes in the mouse and human genome. *Biol. Chem.*, **383**, 725–737.

Yeager,M. (1998) Structure of cardiac gap junction intercellular channels. *J. Struct. Biol.*, **121**, 231–245.

Zhang,J.T. and Nicholson,B.J. (1994) The topological structure of connexin 26 and its distribution compared to connexin 32 in hepatic gap junctions. *J. Membr. Biol.*, **139**, 15–29.

Received November 16, 2001; revised April 12, 2002; accepted May 22, 2002